Gluon saturation and pseudo-rapidity distributions of charged hadrons at RHIC energy regions*

WEI Xin-Bing(魏新兵)[1] FENG Sheng-Qin(冯笙琴)[1,2,3;1)]

[1] College of Science, China Three Gorges University, Yichang 443002, China
[2] Key Laboratory of Quark and Lepton Physics (Huazhong Normal University), Ministry of Education，Wuhan 430079, China
[3] School of Physics and Technology, Wuhan University, Wuhan 430072, China

Abstract: We modified the gluon saturation model by rescaling the momentum fraction according to saturation momentum and introduced Cooper-Frye hydrodynamic evolution to systematically study the pseudo-rapidity distributions of final charged hadrons at different energies and different centralities for Au-Au collisions in relativistic heavy-ion collisions at the BNL Relativistic Heavy Ion Collider (RHIC). The features of both gluon saturation and hydrodynamic evolution at different energies and different centralities for Au-Au collisions are investigated in this paper.

Key words: color glass condensate，gluon saturation, hydrodynamic evolution

PACS: 25.75.-q, 25.75.Ag, 25.75.Nq **DOI:** 10.1088/1674-1137/36/11/006

1 Introduction

After several years of RHIC operation, a wealth of experimental results on multi-particle production have become available. It appears that the data on hadron multiplicity and its energy, centrality, and rapidity dependence so far are consistent with the approach [1, 2] based on the ideas of gluon saturation [3, 4] or the color glass condensate (CGC) [5–10].

CGC describes a state that at very high energies, a new form of matter is created: a dense condensate of gluons. In a hadron, the constituents are the valence quarks, gluons, and sea quarks. As the collision energy increases, the gluons in a hadron will radiate new gluons and the gluons take a dominate state in the hadron. As a matter of fact, the number of a certain kind of gluons will not increase for ever in a fixed hadron, and then it trends toward a constant. That is gluon saturation.

There exists a lot of extensive work [1–10] on the description of gluon productions in nuclear collisions in the saturation regime where nonlinear effects become important. Perturbative solutions for the collision of two nuclei in the MV model were obtained in Refs. [7–17]. However, those solutions are limited for the relatively high momentum and cannot be used for the calculation of total gluon multiplicities. One of our purposes in this paper is to investigate the rapidity dependence of final hadrons.

Here we should mention a novel gluon saturation model proposed by Kharzeev, Levin, and Nardi (KLN) [1, 2, 18, 19] to discuss the gluon saturation mechanism and calculate the gluon rapidity distribution. An analytical scaling function which embodies the predictions of high density QCD on the energy, centrality and rapidity dependences of hadron multiplicities in nuclear collisions are proposed in this model [1, 2, 18, 19]. In Ref. [1], it is found that the simplified KLN model could fit the central rapidity distribution well ($-4.5 < \eta < 4.5$) as shown in Fig. 1(a) when compared with the RHIC data [20]. But if we extend the simplified KLN model to fit the distribution of the full rapidity region as shown in Fig. 1(b), it is found that the simplified KLN model jumps abruptly at the large rapidity region. In order to solve the problem, we modified the gluon satura-

Received 21 January 2012

* Supported by National Natural Science Foundation of China (10975091), Excellent Youth Foundation of Hubei Scientific Committee (2006ABB036) and Education Commission of Hubei Province of China (Z20081302)

1) Corresponding author. E-mail: fengsq@ctgu.edu.cn

©2012 Chinese Physical Society and the Institute of High Energy Physics of the Chinese Academy of Sciences and the Institute of Modern Physics of the Chinese Academy of Sciences and IOP Publishing Ltd

tion model by rescaling the momentum fraction according to saturation momentum Q_s. Then we introduce the Cooper-Frye hydrodynamic evolution to study the rapidity distributions of final charged hadrons in this paper.

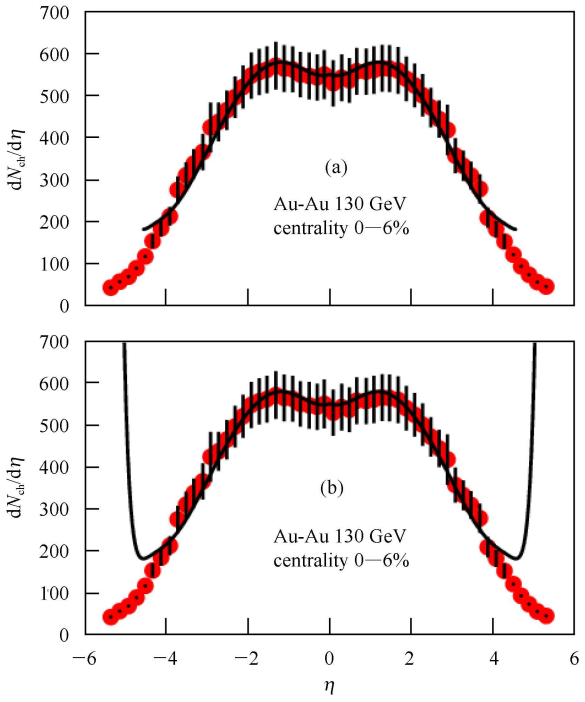

Fig. 1. The charged hadron pseudo-rapidity distribution of the central collision at $\sqrt{s_{\rm NN}}$= 130 GeV. Fig. 1(a) comes from the simplified KLN model [1] and Fig. 1(b) extends the simplified KLN model [1] to a large rapidity region. The real lines are the calculated results and the experimental results are from data of Phobos/RHIC [20].

This paper is organized as follows. In Section 2, we give a detailed review of the modified gluon saturation model for the initial condition, and then introduce the Cooper-Frye hydrodynamic evolution. The comparison and analysis of charged hadron pseudo-rapidity distribution at RHIC with the results of the model are given in Section 3. Section 4 gives a summary and conclusions.

2 The modified gluon saturation model connecting with hydrodynamics

As mentioned above, color glass condensate creates a dense condensate of gluons [21]. Color: the gluons are colored. Glass: there is a very high density of massless gluons. Condensate: these gluons can be packed until their phase space density is so high that interactions prevent more gluon occupation. With increasing energy, this forces the gluons to occupy higher momenta, so that the coupling becomes weak. The gluon density saturates at a value of order $\alpha_s \ll 1$, corresponding to a multiparticles state which is a Bose condensate.

One can define the transverse momentum of gluon saturation as the saturation momentum Q_s (saturation scale) at very high collision energy. The saturation scale can be estimated as [11–17]:

$$Q_s^2 = \alpha_s N_c \frac{1}{\pi R^2}\frac{{\rm d}N}{{\rm d}y}. \tag{1}$$

KLN [1, 2] discussed gluon saturation of two identical nuclei collision situations and introduced two auxiliary variables

$$Q_{s,\min}(y,\sqrt{s_{\rm NN}}) = \min\{Q_s(A;x_1),\ Q_s(A;x_2)\}, \tag{2}$$

$$Q_{s,\max}(y,\sqrt{s_{\rm NN}}) = \max\{Q_s(A;x_1),\ Q_s(A;x_2)\}. \tag{3}$$

From Eq. (2) and Eq. (3), when y=0, we can find $Q_{s,\max} = Q_{s,\min}$ and when $y > 0$ (or $y < 0$), $Q_{s,\min} = Q_s(A,\mp y,\sqrt{s_{\rm NN}})$, $Q_{s,\max} = Q_s(A,\pm y,\sqrt{s_{\rm NN}})$. Then one can define [1, 2]

$$\begin{aligned} Q_{s,\min} &= Q_s(A,-y,\sqrt{s_{\rm NN}}) \\ &= Q_s(\sqrt{s_{\rm NN0}})(\sqrt{s_{\rm NN}}/\sqrt{s_{\rm NN0}})^{\lambda/2}{\rm e}^{-|y|/2} \\ &= Q_s(s_{\rm NN}){\rm e}^{-|y|/2}, \end{aligned} \tag{4}$$

$$\begin{aligned} Q_{s,\max} &= Q_s(A,y,\sqrt{s_{\rm NN}}) \\ &= Q_s(\sqrt{s_{\rm NN0}})(\sqrt{s_{\rm NN}}/\sqrt{s_{\rm NN0}})^{\lambda/2}{\rm e}^{|y|/2} \\ &= Q_s(s_{\rm NN}){\rm e}^{|y|/2}, \end{aligned} \tag{5}$$

where $\sqrt{s_{\rm NN0}}$=130 GeV, $Q_s^2(\sqrt{s_{\rm NN0}}) = 2.05$ [1, 2], and λ the growth of the gluon structure functions at small x in deep-inelastic scattering. The HERA data are fitted with $\lambda \approx 0.25-0.3$ [22–24].

The differential cross section of gluon production in A-A collision can be written down as [3, 4]:

$$\begin{aligned} E\frac{{\rm d}\sigma}{{\rm d}^3p} &= \frac{4\pi N_c}{N_c^2-1}\frac{1}{p_t^2}\int {\rm d}k_t^2 \alpha_s \left[\varphi_{A_1}(x_1,k_t^2)\right. \\ &\quad \left.\times\varphi_{A_2}(x_2,(p-k)_t^2)\right], \end{aligned} \tag{6}$$

where k_t and p_t are the transverse momentums of a parton in a hadron before collision and of the produced gluon, respectively, and α_s is the running coupling coefficient and takes a smaller value. The unintegrated gluon distribution $\varphi(x,k_t^2)$ describes the probability of finding a gluon with a given x and

transverse momentum $k_{\rm t}$ inside the nucleus A [1, 2, 18, 19]. The gluon saturation function can be given by

$$xG(x,p_{\rm t}^2)=p_{\rm t}^2\int {\rm d}k_{\rm t}^2\varphi(x,k_{\rm t}^2). \tag{7}$$

The expression shows that gluon saturation function is the average value of $\varphi(x,k_{\rm t}^2)$ at a given transverse momentum region. Therefore, the multiplicity distribution of gluons is [1, 2]

$$\frac{{\rm d}N_{\rm g}}{{\rm d}y}=\frac{1}{S}\int {\rm d}^2p_{\rm t}\left(E\frac{{\rm d}\sigma}{{\rm d}^3p}\right), \tag{8}$$

S is either the inelastic cross section for the minimum bias multiplicity, or a fraction of it corresponding to a specific centrality cut [1, 2].

KLN [1] gave the gluon distribution by considering two integration regions: $k_{\rm t}\ll p_{\rm t}$ and $\left|\vec{p}_{\rm t}-\vec{k}_{\rm t}\right|\ll p_{\rm t}$; this leads to

$$\begin{aligned}\frac{{\rm d}N_{\rm g}}{{\rm d}y} &= \frac{1}{S}\int {\rm d}^2p_{\rm t}\left(E\frac{{\rm d}\sigma}{{\rm d}^3p}\right)=\frac{1}{S}\frac{4\pi N_{\rm c}\alpha_{\rm s}}{N_{\rm c}^2-1}\\ &\times\int\frac{{\rm d}^2p_{\rm t}}{p_{\rm t}^2}\left[\varphi_{A_1}(x_1,p_{\rm t}^2)p_{\rm t}\int {\rm d}k_{\rm t}^2\varphi_{A_2}(x_2,k_{\rm t}^2)\right.\\ &\left.+\varphi_{A_2}(x_2,p_{\rm t}^2)p_{\rm t}\int {\rm d}k_{\rm t}^2\varphi_{A_1}(x_1,k_t^2)\right]\\ &= \frac{1}{S}\frac{4\pi N_{\rm c}\alpha_{\rm s}}{N_{\rm c}^2-1}\int_0^\infty\frac{{\rm d}^2p_{\rm t}}{p_{\rm t}^4}x_2G_{A_2}(x_2,p_{\rm t}^2)x_1G_{A_1}(x_1,p_{\rm t}^2).\end{aligned} \tag{9}$$

The gluon distribution takes as [1, 2, 18, 19],

$$xG(x,p_{\rm t}^2)=\begin{cases}\dfrac{\kappa}{\alpha_{\rm s}(Q_{\rm s}^2)}Sp_{\rm t}^2(1-x)^4 & p_{\rm t}<Q_{\rm s}(x),\\ \dfrac{\kappa}{\alpha_{\rm s}(Q_{\rm s}^2)}SQ_{\rm s}^2(1-x)^4 & p_{\rm t}>Q_{\rm s}(x),\end{cases} \tag{10}$$

According to Refs. [18, 19], the $p_{\rm t}$ integration is divided into three regions:
(1) $p_{\rm t}<Q_{\rm s,min}<Q_{\rm s,max}$, in this region, both parton densities for the two nuclei are in the saturation region.
(2) $Q_{\rm s,min}<p_{\rm t}<Q_{\rm s,max}$, in this region, one nucleus is in the saturation region, and the other one is in the normal DGLAP region .
(3) $p_{\rm t}>Q_{\rm s,max}>Q_{\rm s,min}$, in this region the parton densities in both nuclei are in the DGLAP evolution region.

The gluon distribution is given as follows [1, 2]:

$$\begin{aligned}\frac{{\rm d}N_{\rm g}}{{\rm d}y} &= \frac{N_{\rm c}\kappa^2\beta_0}{N_{\rm c}^2-1}\frac{N_{\rm part}}{Q_{\rm s0}^2}\ln\frac{Q_{\rm s,min}^2}{\Lambda_{\rm QCD}^2}\left\{\int_0^{Q_{\rm s,min}}(1-x_1)^4(1-x_2)^4{\rm d}^2p_{\rm t}+Q_{\rm s,min}^2\int_{Q_{\rm s,min}}^{Q_{\rm s,max}}\frac{1}{p_{\rm t}^2}(1-x_1)^4(1-x_2)^4{\rm d}^2p_{\rm t}\right.\\ &\left.+Q_{\rm s,min}^2Q_{\rm s,max}^2\int_{Q_{\rm s,max}}^{\infty}\frac{1}{p_{\rm t}^4}(1-x_1)^4(1-x_2)^4{\rm d}^2p_{\rm t}\right\},\end{aligned} \tag{11}$$

where $\beta_0=11-\dfrac{2}{3}N_{\rm f}$, $N_{\rm f}=3$.

The KLN model [1] realized that the gluon distributions are the final hadron distributions. This was based on the assumption that the final state interactions did not change the multiplicities of partons resulting from the early stages of the process significantly [1, 2].

In the KLN model [1], they defined the momentum fraction as follows:

$$x_1=\frac{p_{\rm t}}{\sqrt{s_{\rm NN}}}{\rm e}^{-y},\quad x_2=\frac{p_{\rm t}}{\sqrt{s_{\rm NN}}}{\rm e}^{y}. \tag{12}$$

Here we should say a few words about Fig. 2. Even if we use the integrated Eq. (9) and Eq. (11) to fit the PHOBOS experimental data of the RHIC energy region, we find that the integrated KLN model cannot fit well with the experimental results at a large pseudo-rapidity region, as shown in Fig. 2. In order to solve this problem, it is assumed that the momentum fraction at Eq. (9) should depend on the structure function and saturation momentum of the collision nuclei in the saturation region.

Here we rescale the momentum fraction according to the saturation momentum:

$$\begin{aligned}x_1 &= \frac{Q_{\rm s,min}}{\sqrt{s_{\rm NN}}}=\frac{p_{\rm t}}{\sqrt{s_{\rm NN}}}{\rm e}^{-|y|/2},\\ x_2 &= \frac{Q_{\rm s,max}}{\sqrt{s_{\rm NN}}}=\frac{p_{\rm t}}{\sqrt{s_{\rm NN}}}{\rm e}^{|y|/2}.\end{aligned} \tag{13}$$

After carefully studying the KLN model and the recent PHOBOS experimental data, we propose to rescale the fraction momentum according to the saturation momentum, and introduce the CGC as initial condition to connect with Cooper-Frye hydrodynamic evolution to study the pseudo-rapidity distributions of final charged hadrons.

At RHIC, two collider nuclei will be Lorentz contracted. At the moment after collision, they will experience a quantum fluctuation ($\tau\sim 0-0.1$ fm/c), density fluctuation, and thermalization ($\tau\sim 0.1$–1 fm/c). For the central collision of big nuclei, fluid near the collision axis moves longitudinally and homoge-

neously. We can take the two nuclei as two thin pancakes, the fluid midway between the receding pancakes remains at rest [25, 26].

We assume that the system of gluons initially produced from the CGC reaches a kinematically as well as chemically local equilibrate state at a short time scale. We further assume that during thermalization, the shape of the rapidity distribution is not changed. Thus, we take the initial conditions from gluon distribution obtained in the previous subsection based on the CGC.

We adopt Bjorken's assumption [25] that $y=\eta_{\rm s}$, where y is the energy-momentum rapidity, and $\eta_{\rm s}$ is the space-time rapidity

$$\left(\eta_{\rm s}=\frac{1}{2}\ln\frac{x^+}{x^-}\right).$$

Due to Formula (13), the gluon density [25] at point (τ_0,y) is

$$n_{\rm g}(\tau_0,y)=\frac{{\rm d}N_{\rm g}}{\tau_0{\rm d}y}, \tag{14}$$

where τ_0 is the initial time. Let us recall the relations among thermodynamic variables, i.e., temperature T and related number density $n(\tau_0,y)$ for the massless free parton system:

$$n(\tau_0,y)=(3/4g_{\rm q}+g_{\rm g})\frac{\zeta(3)}{\pi^2}T^3(\tau_0,y), \tag{15}$$

then

$$T(\tau_0,y)=\left[\frac{\pi^2 n(\tau_0,y)}{43\zeta(3)}\right]^{1/3}, \tag{16}$$

where $g_{\rm q}=2N_{\rm c}N_{\rm s}N_{\rm f}=36$, $g_{\rm g}=2(N_{\rm c}^2-1)=16$, $\zeta(3)=1.20206$, color number $N_{\rm c}=3$, flavor number $N_{\rm f}=3$ and spin number $N_{\rm s}=2$. Cooper-Frye assumed that the particle distributions could be described by either a Bose or a Fermi distribution according to the type of the observed particle [27]. The invariant single-particle distribution of gluon in momentum space is

$$E\frac{{\rm d}\sigma}{{\rm d}^3p}=\int_\sigma f(x,p)p^\mu{\rm d}\sigma_\mu=\frac{g}{(2\pi)^3}\int\frac{p^\mu{\rm d}\sigma_\mu}{{\rm e}^{E/T}-1}. \tag{17}$$

Adopting a cylinder with radius R and length $2\eta_0$ in the case of no transverse fluid and flat temperature profile, we can get

$${\rm d}\sigma_\mu=\int{\rm d}\eta_{\rm s}\pi R^2\tau(\cosh\eta_{\rm s},0_\perp,\sinh\eta_{\rm s}). \tag{18}$$

In the midway $\eta_{\rm s}\approx0$, therefore

$$p^\mu{\rm d}\sigma_\mu=p^0\pi R^2\tau{\rm d}\eta_{\rm s}, \tag{19}$$

The rapidity distribution is:

$$\begin{aligned}\frac{{\rm d}N_{\rm ch}}{{\rm d}y} &= \frac{g}{(2\pi)^3}\int E\frac{{\rm d}N^3}{{\rm d}^3p}{\rm d}^2p_{\rm t}\\ &= \frac{g}{(2\pi)^3}\int_{-\eta_0}^{\eta_0}{\rm d}\eta_{\rm s}\cdot\int_0^\infty{\rm d}p_{\rm t}p_{\rm t}^2\pi R^2\tau\\ &\quad\times\cosh(\eta_{\rm s}-y)f(\vec{p}),\end{aligned} \tag{20}$$

where

$$f(\vec{p})=\frac{1}{\exp\left[p_{\rm t}\cosh(\eta_{\rm s}-y)/T\right]-1}.$$

Consequently,

$$\begin{aligned}\frac{{\rm d}N_{\rm ch}}{{\rm d}y} &= \frac{g}{(2\pi)^3}4\pi^2R^2\tau T^3[\tanh(y+\eta_0)\\ &\quad-\tanh(y-\eta_0)].\end{aligned} \tag{21}$$

Substituting Formulas (14) and (16) into (21), we obtain the following formula of rapidity distribution of final charged hadrons as follows:

$$\frac{{\rm d}N_{\rm ch}}{{\rm d}y}=\frac{\pi R^2g}{86\zeta(3)}\cdot\frac{\tau}{\tau_0}\cdot\frac{{\rm d}N_{\rm g}}{{\rm d}y}\times[\tanh(y+\eta_0)-\tanh(y-\eta_0)], \tag{22}$$

where degeneracy $g=\frac{3}{4}g_{\rm q}+g_{\rm g}$, η_0 is the kinematical range of collective flow in the longitudinal direction of nuclear-nuclear collisions [28–34], R is the radius of the phase space of cylinder and τ is the "proper time" defined as [25]:

$$\tau=\sqrt{t^2-z^2}. \tag{23}$$

From (11) and (22) we can get the rapidity distribution of charged hadrons as follows:

$$\begin{aligned}\frac{{\rm d}N_{\rm ch}}{{\rm d}y} &= \frac{\pi R^2g}{86\zeta(3)}\cdot\frac{\tau}{\tau_0}\frac{N_{\rm c}\kappa^2\beta_0}{N_{\rm c}^2-1}\frac{N_{\rm part}}{Q_{\rm s0}^2}\\ &\quad\times\ln\frac{Q_{\rm s,min}^2}{\Lambda_{\rm QCD}^2}\left\{\int_0^{Q_{\rm s,min}}(1-x_1)^4(1-x_2)^4{\rm d}^2p_{\rm t}\right.\\ &\quad+Q_{\rm s,min}^2\int_{Q_{\rm s,min}}^{Q_{\rm s,max}}\frac{1}{p_{\rm t}^2}(1-x_1)^4(1-x_2)^4{\rm d}^2p_{\rm t}\\ &\quad+Q_{\rm s,min}^2Q_{\rm s,max}^2\int_{Q_{\rm s,max}}^\infty\frac{1}{p_{\rm t}^4}(1-x_1)^4(1-x_2)^4\\ &\quad\left.\times{\rm d}^2p_{\rm t}\right\}\times[\tanh(y+\eta_0)-\tanh(y-\eta_0)].\end{aligned} \tag{24}$$

The pseudo-rapidity distribution takes the following form:

$$\frac{{\rm d}N}{{\rm d}\eta}=\sqrt{1-\frac{m^2}{m_{\rm t}^2\cosh^2y}}\frac{{\rm d}N}{{\rm d}y}, \tag{25}$$

here $y = 0.5 \ln \frac{\sqrt{p_t^2 \cosh^2 \eta + m^2} + p_t \sinh \eta}{\sqrt{p_t^2 \cosh^2 \eta + m^2} - p_t \sinh \eta}$, $m_t^2 = p_t^2 + m^2$, $p_t = Q_s$.

3 The pseudo-rapidity distributions of charged hadrons

The study of relativistic heavy-ion collisions is the only known method of creating and studying, in the laboratory, systems with hadronic or partonic degrees of freedom at extreme energy and matter density over a significant volume. It is for this reason that in recent years such studies have attracted much experimental and theoretical interest, in particular with the likelihood that, at higher energies, a new state of QCD matter is created.

The PHOBOS Collaboration, working at RHIC, has presented considerable experimental data [35] of different energies and different centralities of Au-Au collisions at $\sqrt{s_{NN}}$=19.6, 62.4,130 and 200 GeV, respectively. This extensive body of data on the global properties of particle production in heavy-ion collisions can be used to provide an insight into both our understanding of the mechanisms of particle production and the properties of matter that exist at extremes of energy and matter densities. In this paper, we will use the modified gluon saturation model to study the rapidity distributions of final charged hadrons.

The results are presented in Fig. 2. It is found that the calculation results from our model are consistent with those of the experimental data, especially at relatively large collision energies of $\sqrt{s_{NN}}$=130 and 200 GeV. It is suggested that the modified gluon saturation model prefers the relatively large collision energies of $\sqrt{s_{NN}}$=130 and 200 GeV to the relatively low collision energies of $\sqrt{s_{NN}}$=19.6, 62.4 GeV. It is suggested that the large collision energy of RHIC could easily reach the situation of gluon saturation and hydrodynamic evolution.

The charged hadron pseudo-rapidity distributions are shown in Fig. 3 (a), (b), (c) and (d) for Au-Au collisions at different energies and different centralities of 0–3%, 3%–6%, 35%–40% and 40%–45%, respectively. It is shown that the modified gluon saturation model tends to explain the central collision better

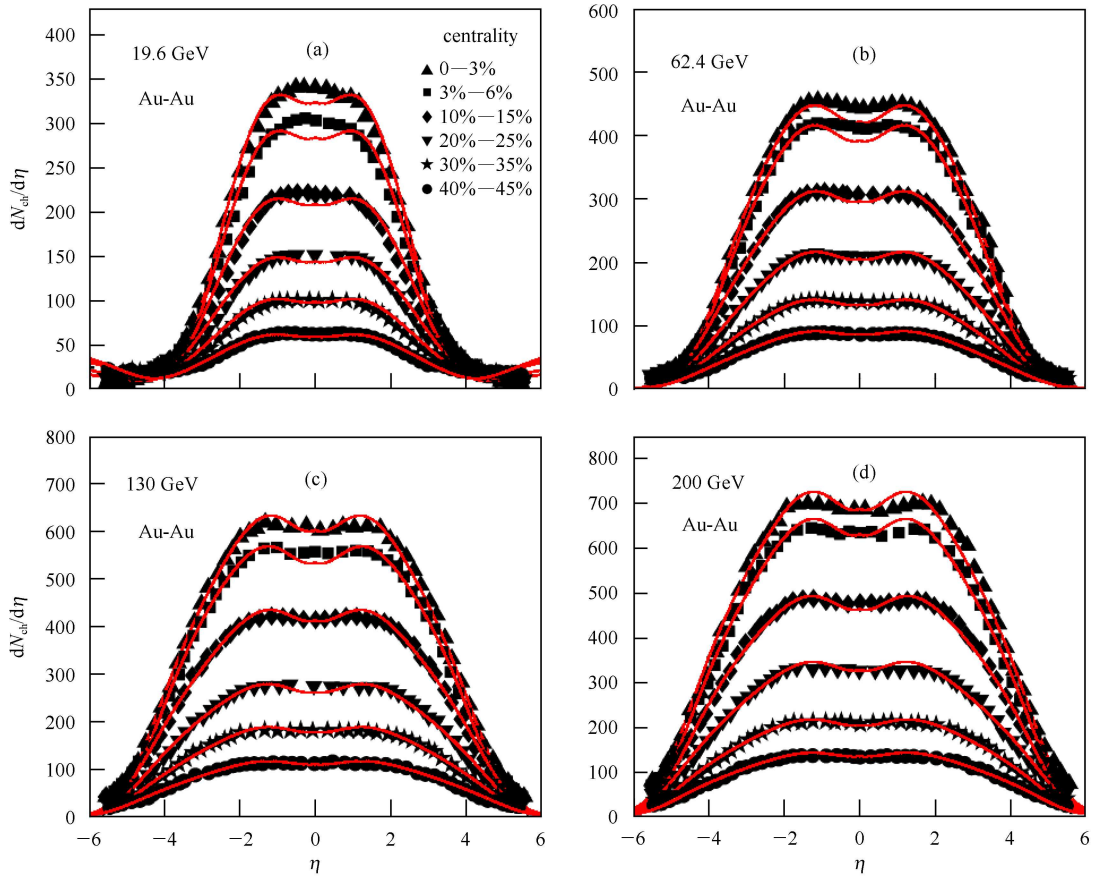

Fig. 2. The charged hadron pseudo-rapidity distributions are shown in Fig. 2(a), (b), (c) and (d) for Au-Au collisions at different collision energies $\sqrt{s_{NN}}$=19.6, 62.4, 130 and 200 GeV respectively. The solid lines are the results from our modified gluon saturation model. The experimental data are given by PHOBOS [35].

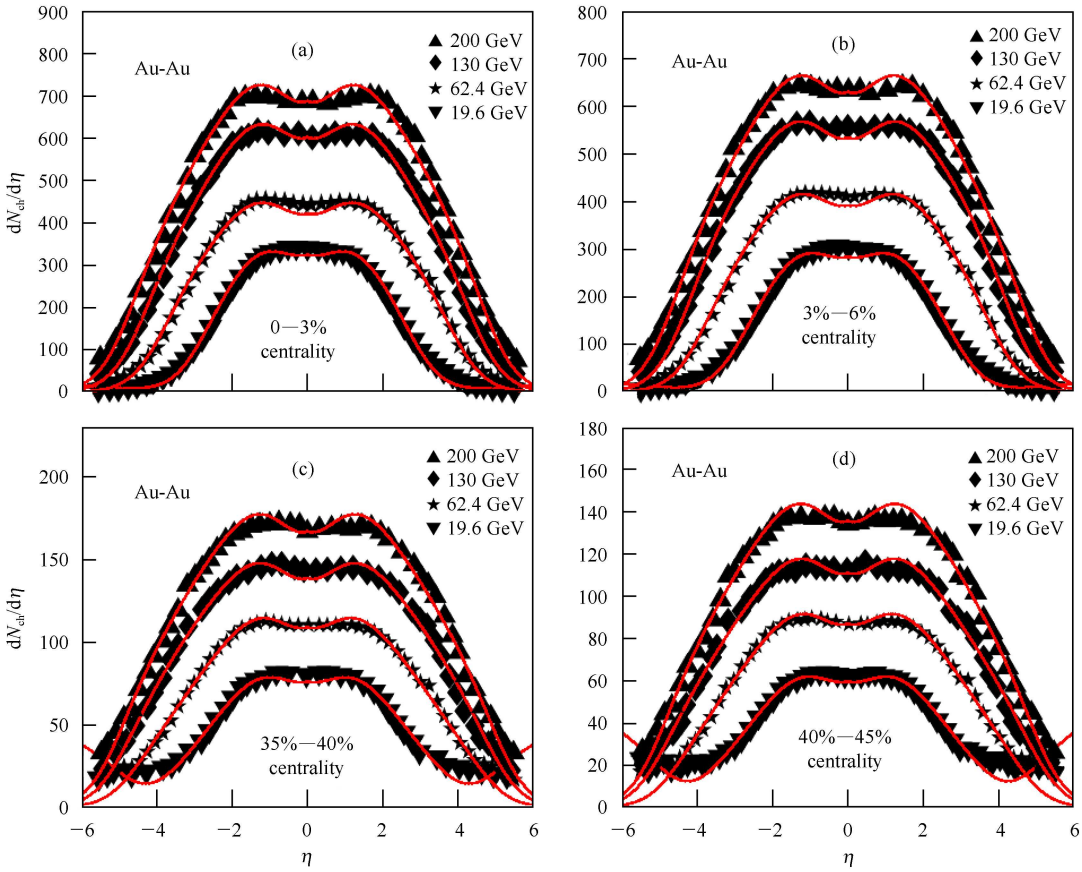

Fig. 3. The charged hadron pseudo-rapidity distributions are shown in Fig. 3 (a), (b), (c) and (d) for Au-Au collisions at different energies and different centralities of 0–3%, 3%–6%, 35%–40% and 40%–45%, respectively. The solid lines are the results from our modified gluon saturation model. The experimental data are given by PHOBOS [35].

than that of the peripheral collision. The experimental data are given by PHOBOS [35]. It is suggested that the central collision system could easily reach the situation of gluon saturation and hydrodynamic evolution.

Here, we should say a few words about η_0, according to the Bjorken evolutionary picture η_0 is the boost invariance limitation of thermalization source. Combining with this paper, we realize that η_0 is the rapidity limitation of emission source, where the final charged hadrons hydrodynamic evolution is from. It seems reasonable to take the limitation η_0 of the emission source as the thermalization limitation of the abundance of saturation gluons.

By fitting with the PHOBOS data [34], we get the dependence of the limitations η_0 on $\ln\sqrt[4]{s_{\rm NN}}$ at different centrality of 0–3%, 3%–6%, 35%–40% and 40%–45%, respectively, at Fig. 4 (a), (b), (c) and (d). The different linear dependences of centralities of 0–3%, 3%–6%, 35%–40% and 40%–45%, respectively, on CMS collision energies can be given as follows:

$$\eta_0 = 1.63\ln\sqrt[4]{s_{\rm NN}} + 0.42 \text{ (centrality 0–3\%)}, \quad (26)$$

$$\eta_0 = 1.49\ln\sqrt[4]{s_{\rm NN}} + 0.70 \text{ (centrality 3\%–6\%)}, \quad (27)$$

$$\eta_0 = 0.90\ln\sqrt[4]{s_{\rm NN}} + 2.70 \text{ (centrality 35\%–40\%)}, \quad (28)$$

$$\eta_0 = 0.87\ln\sqrt[4]{s_{\rm NN}} + 2.76 \text{ (centrality 40\%–45\%)}. \quad (29)$$

From the linear $\ln\sqrt[4]{s_{\rm NN}}$ relationship, we can predict the η_0 at LHC $\sqrt{s_{\rm NN}}$=5500 GeV at a certain centralities. Until now, we have not found the LHC data of the rapidity distributions of produced hadrons in the central region or full rapidity region of Pb-Pb collisions. We will discuss the rapidity distribution at the LHC energy region in our next work.

4 Summary and conclusion

As follows, we will discuss the space–time picture of ultra-relativistic nuclear collisions when presenting

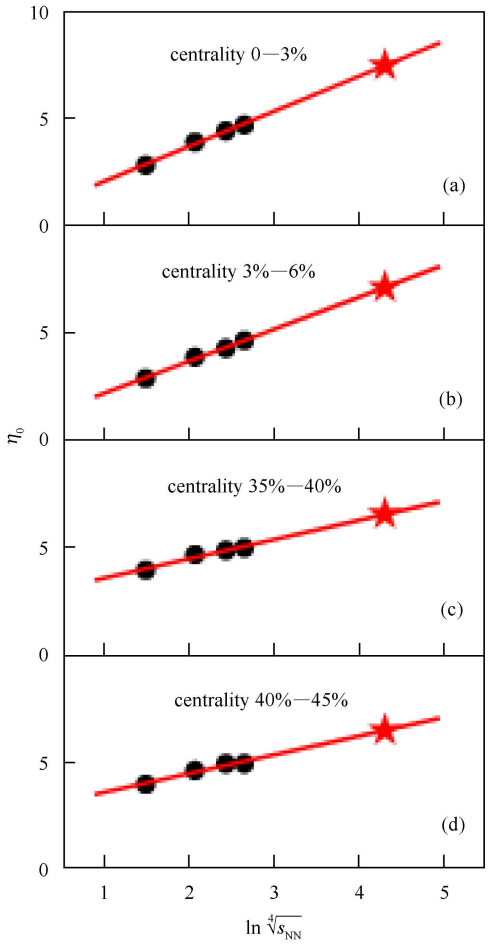

Fig. 4. The dependence of the limitation η_0 of a thermalization region with $\ln \sqrt[4]{s_{NN}}$ at different centralities of 0–3%, 3%–6%, 35%–40% and 40%–45%. The star ($\star$) is the results of our model's prediction of LHC $\sqrt{s_{NN}}$= 5500 GeV.

the CGC physics. Heavy ion collisions at ultra-relativistic energies are shown in Fig. 5 as the collision of two sheets of colored glass [12, 21]. The nuclei appear as sheets at ultra-relativistic energies because of Lorentz contraction. The CGC gluons are shown as vectors which represent the polarization of the gluons, and by colors corresponding to the various colors of gluons.

At ultra-relativistic energies, these sheets pass through one another. What they leave is the melting colored glass, which eventually materializes as quarks and gluons. These quarks and gluons would naturally form in their rest frame on some natural microphysics time scale. For the saturated color glass this proper formation time scale τ_0, is of the order of the inverse saturation momentum. At RHIC, each is contracted by a gamma factor 100, in the center of mass frame at RHIC. For particles with a large momentum or rapidity along the beam axis, this time scale is Lorentz dilated. This means that the slow (smaller rapidity) particles are produced first towards the center of the collision regions and the fast (larger rapidity) particles are produced later further away from the collision region. This means that the matter produced at RHIC, like the universe in cosmology, is born expanding. One important difference is that the "mini-bang" at RHIC is born with one-dimensional flow along the collision axis, while the big bang is three-dimensional. This is shown in Fig. 6.

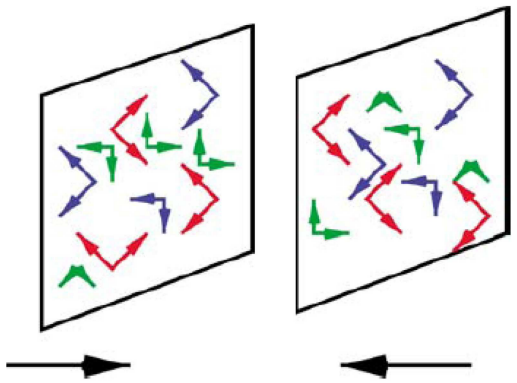

Fig. 5. The collision of two sheets of colored glass [21].

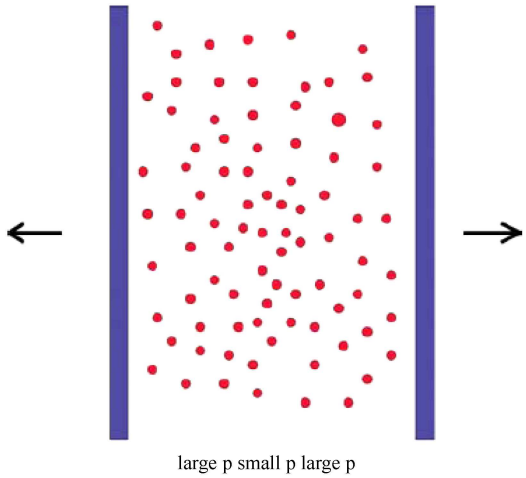

Fig. 6. Particles being produced after the collision of two nuclei.

As this system expands, it cools. The produced quarks and gluons may thermalize. If local equilibrium is reached early with $\tau_{eq} < 1$ fm/c, then the QGP can develop collective flow according to the laws of hydrodynamics. Eventually, all the quarks and gluons must become confined into hadrons before being detected.

We modified the gluon saturation model by rescaling the momentum fraction according to the saturation momentum, and introduced the Cooper-Frye hydrodynamic evolution to study the pseudo-rapidity

distributions of final charged hadrons in this paper. It is found that our new modified gluon saturation model can fit well the full rapidity region of the recent published PHOBOS results at RHIC at different centralities and different energies.

From the discussions, we can find that our calculation results are consistent with those of the experimental data, especially at relatively large collision energies of $\sqrt{s_{\rm NN}}$=130 and 200 GeV. It is suggested that the RHIC's large collision energy can easily reach the situation of gluon saturation and hydrodynamic evolution.

By comparing with experimental data, we also find that the gluon saturation model prefers central collisions to peripheral collisions. It is suggested that central collisions at RHIC can easily reach the situation of gluon saturation and hydrodynamic evolution than that of peripheral collisions. By connecting with hydrodynamic evolution, we can find that the limitations η_0 of the thermalization source increase linearly with $\ln\sqrt[4]{s_{\rm NN}}$ at different centralities.

References

1 Kharzeev D, Levin E. Phys. Lett. B, 2001, **523**: 79
2 Kharzeev D, Nardi M. Phys. Lett. B, 2001, **507**: 121
3 Gribov L V, Levin E M, Ryskin M G. Phys. Rep., 1983, **100**: 1
4 Mueller A H, QIU J. Nucl. Phys. B, 1986, **268**: 427
5 Blaizot J P, Mueller A H. Nucl. Phys. B, 1987, **289**: 847
6 McLerran L, Venugopalan R. Phys. Rev. D, 1994, **49**: 2233
7 McLerran L, Venugopalan R. Phys. Rev. D, 1994, **49**: 3352
8 McLerran L, Venugopalan R. Phys. Rev. D, 1994, **50**: 2225
9 Kovchegov Yu V. Phys. Rev. D, 1996, **54**: 5463
10 Kovchegov Yu V, Rischke D H. Phys. Rev. C, 1997, **56**: 1084
11 Kovner A, McLerran L, Weigert H. Phys. Rev. D, 1995, **52**: 3809
12 Kovner A, McLerran L, Weigert H. Phys. Rev. D, 1995, **52**: 6231
13 Gyulassy M, McLerran L. Phys. Rev. C, 1997, **56**: 2219
14 Kovchegov Y V, Rischke D H. Phys. Rev. C, 1997, **56**: 1084
15 Matinyan S G, Müller B, Rischke D H. Phys. Rev. C, 1997, **56**: 2191
16 Matinyan S G, Müller B, Rischke D H. Phys. Rev. C, 1998, **57**: 1927
17 GUO X F. Phys. Rev. D, 1999, **59**: 094017
18 Kharzeev D, Levin E, Nardi M. Phys. Rev. C, 2005, **71**: 054903
19 Kharzeev D, Levin E, Nardi M. Nucl. Phys. A, 2004, **730**: 448
20 Back B et al. (PHOBOS collaboration). Phys. Rev. Lett., 2001, **87**: 102303
21 Miklos Gyulassy , Larry McLerran. Nucl. Phys. A, 2005, **750**: 30
22 Golec-Biernat K, Wüsthof M. Phys. Rev. D, 1999, **59**: 014017
23 Golec-Biernat K, Wüsthof M. Phys. Rev. D, 1999, **59**: 114023
24 Stasto A, Golec-Biernat K, Kwiecinski J. Phys. Rev. Lett., 2001, **86**: 596
25 Bjorken J D. Phys. Rev. D, 1983, **27**: 140
26 Hirano T, Nara Y. Nucl. Phys. A, 2004, **743**: 305
27 Cooper F, Frye G. Phys. Rev. D, 1974, **10**: 186
28 FENG S Q, ZHONG Y. Phys. Rev. C, 2011, **83**: 034908
29 FENG S Q, LIU F, LIU L S. Phys. Rev. C, 2000, **63**: 014901
30 FENG S Q, YUAN X B, SHI Y F. Mod. Phys. Lett. A, 2006, **21**: 663
31 FENG S Q, XIONG W. Phys. Rev. C, 2008, **77**: 044906
32 FENG S Q, YUAN X B. Sci. China Ser. G, 2009, **52**: 198
33 CAI X, FENG S Q, LI Y D, YANG C B, ZHOU D C. Phys. Rev. C, 1995, **51**: 3336
34 FENG S Q. Introduction to Multi-hadron Productions at High Energy Heavy-Ion Collisions. Beijing : Beijing Institute of Technology Press, 2005 (in Chinese)
35 Alver B, Back B B, Baker M D et al. (PHOBOS collaboration). Phys. Rev. C, 2011, **83**: 024913